Scattering of surface plasmons on graphene by abrupt free-carrier generation

A. V. Shirokova, A. V. Maslov, and M. I. Bakunov*
Department of Radiophysics, University of Nizhny Novgorod, Nizhny Novgorod, 603950, Russia

(Received 1 April 2019; published 30 July 2019)

We explore the temporal dynamics of a surface plasmon on a graphene sheet after an abrupt increase of graphene's carrier density. The plasmon is transformed into two frequency-upshifted surface plasmons propagating in the forward and backward directions, transient free-space radiation, and two-stream dc motion of carriers. The two-stream carrier motion carries zero net electric current and therefore does not generate any magnetic field. Nevertheless, it can consume a substantial fraction, up to a half, of the initial plasmon energy in the form of the kinetic energy of the carriers. We revisit the recent claim in the literature that graphene's nonstationarity can amplify plasmons.

DOI: 10.1103/PhysRevB.100.045424

I. INTRODUCTION

Graphene appears to be a promising plasmonic material for the terahertz and infrared frequency ranges due to its capability of supporting low loss and highly confined surface plasmons that can be dynamically tuned by varying the carrier density via electrical gating or optical excitation. These advantages over plasmons in metals make graphene plasmons attractive for a wide range of photonic applications, such as surface-enhanced infrared absorption spectroscopy [1,2], infrared and terahertz photodetectors [3,4], sources [5,6], and modulators [7–9].

The tunability of graphene plasmons is vital for developing graphene-based active plasmonics [10]. By temporally varying the graphene conductivity, one can change the dispersion properties of graphene plasmons and by this means modulate their frequency. Frequency manipulation of optical signals is important, for example, for the wavelength division multiplexing technology in all-optical signal processing [11,12]. Dynamic frequency conversion of light confined in silicon-based photonic structures, both cavities and waveguides, have been experimentally demonstrated by photogeneration of free carriers in silicon [13–18]. For developing high-speed optoelectronic devices, rapid variations of graphene properties are of considerable interest. In particular, ultrafast optical excitation of free carriers in graphene on the scale of a few tens of femtoseconds has been demonstrated [19–21]. The ultrafast dynamics of graphene plasmons after a photoexcitation of carriers has been revealed [22]. Elucidating the role of electron-hole pair creation and hot carrier dynamics on sub-100-fs time scales is currently a subject of intensive study [23,24].

Theoretical understanding of plasmon transformation on a time-varying graphene requires a careful consideration on the basis of nonstationary constitutive relations. Previously, the theory of wave transformation in time-varying media has been mainly developed for the waves in bulk materials, such as dielectrics or plasmas [25–29]. The transformation of surface waves was investigated in the geometries of plasma half-space [30–32] or plasma layers [31,33], both for slow [31] and rapid [30,32,33] plasma density variations. It was found that medium nonstationarity can give rise to specific effects such as frequency shifting, reflection at the temporal boundaries, temporal scattering of surface waves to bulk radiation, and generation of self-consistent distributions of static magnetic field and dc currents (the so-called free-streaming modes) in plasma. These effects, however, were not considered for the waves guided by two-dimensional structures, such as graphene sheets.

The problem of graphene plasmon transformation by time modulation of graphene's free-carrier density was addressed very recently in Refs. [34] and [35]. The most salient prediction of these works is that nonstationarity can amplify plasmons by imparting energy to them. In Ref. [34], the plasmon amplification occurs if the carrier density abruptly decreases. In Ref. [35], on the contrary, the amplification was predicted for a carrier density increase.

In a more recent paper [36], however, the claim of plasmon amplification, made in Ref. [34] for the carrier density decrease, was refuted and the origin of the mistake was pointed out. Namely, the approach of Ref. [34] is based on the continuity of the plasmon's magnetic field and its time derivative at the temporal discontinuity and on a simultaneous neglect of the transient bulk radiation. The transient radiation is indeed negligible in the quasistatic regime studied in Ref. [34]. The plasmon's magnetic field, however, is also negligible, and using the continuity of this field and its derivative without including transient radiation is incorrect. For a correct consideration, one should use the initial conditions for the dominant components of the plasmon, i.e., its in-plane electric field and surface current [36].

In Ref. [35], the consideration is also limited by the quasistatic approximation but, unlike Ref. [34], other initial conditions, namely, the continuity of the plasmon's electric and magnetic fields at the temporal discontinuity, are used without any justification. Due to different initial conditions, the results of Refs. [34] and [35] contradict each other. Moreover, as was

*bakunov@rf.unn.ru

shown in Ref. [36], the results of Ref. [35] for the carrier density decrease are also incorrect.

Unlike Refs. [34] and [35], the approach of Ref. [36] is based on accurately solving the Maxwell equations with an assumption that a decrease of the carrier density (the carrier removal) leaves the current of the remaining carriers unchanged. By using this approach, it was shown that the total energy of the scattered (transmitted and reflected) plasmons and transient bulk radiation is smaller than the initial plasmon energy by the amount of the kinetic energy of the removed carriers.

In this paper, we extend the approach of Ref. [36] to the problem of graphene plasmon scattering by an abrupt increase of carrier density. As constitutive relations, we use the time-domain Drude equations for the background and newly created carriers. Based on accurate solution of the Maxwell equations, our consideration is not limited by the quasistatic approximation; nevertheless we analyze the quasistatic regime in detail because of its practical importance. We also carefully study the energy balance in the system and show that the plasmon amplification does not exist at the carrier density temporal increase, in contrast to the prediction of Ref. [35]. On the contrary, we show that a part of the initial plasmon energy is consumed by a specific two-stream dc motion of carriers, thus reducing the energy of the scattered plasmons. We explain the origin of the mistake in Ref. [35].

Importantly, the formulas for the amplitudes and energies of the scattered plasmons we obtain below are different from those in Ref. [36] for an abrupt carrier density decrease. This refutes the view [34,35] that both an increase and decrease in carrier density can be described by the same universal formulas.

II. MODEL AND BASIC EQUATIONS

We consider an infinite graphene sheet placed at the plane $y = 0$ (Fig. 1) and surrounded by a dielectric with permittivity ε (in numerical results we set $\varepsilon = 1$). Graphene is characterized in terms of the Drude model by a frequency-dependent complex (for fields $\propto e^{i\omega t}$) surface conductivity

$$\sigma(\omega) = -ic\Omega/(2\pi\omega), \quad \Omega = 2e^2 E_F/\hbar^2, \tag{1}$$

conveniently expressed through the frequency parameter Ω, which is proportional to the Fermi energy E_F (c is the speed of light, e is the electron charge, and $\hbar$ is the reduced Planck

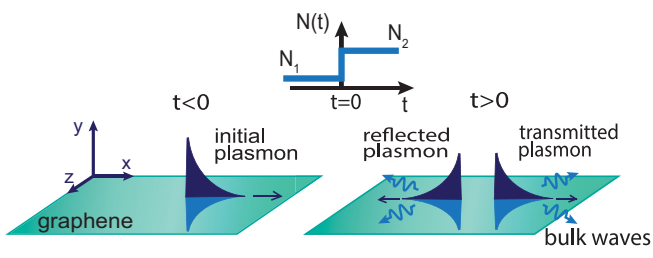

FIG. 1. Schematic view of a surface plasmon propagating along a graphene sheet at $t < 0$ and scattered to reflected and transmitted plasmons and bulk radiation at $t > 0$. Inset: Time dependence of the graphene carrier density.

constant). Since the Fermi level depends on the electron surface density N as $E_F = \hbar v_F \sqrt{\pi N}$, with $v_F \approx 10^6$ m/s the Fermi velocity of graphene, the parameter Ω scales as $\Omega \propto \sqrt{N}$. For example, for a typical doping, $N = 10^{13}$ cm^{-2}, the Fermi energy is $E_F \approx 370$ meV and Ω resides in the subterahertz regime: $\Omega \approx 0.276 \times 10^{12}$ s^{-1}.

Drude-like Eq. (1) neglects the interband transitions and temperature effects [37,38]. This is a good approximation for highly doped graphene with $E_F \gg k_B T$ (k_B is the Boltzmann constant, T is the temperature, $k_B T \approx 26$ meV at $T \approx 300$ K) and $E_F > \hbar\omega/2$ ($\hbar\omega \approx$ 4–400 meV for the terahertz and mid-infrared frequency ranges). For the sake of clarity, we omitted collisions in Eq. (1). The presence of carrier collisions will lead to a gradual damping of the scattered surface plasmons but should not significantly affect the fields immediately after the rapid carrier density increase.

We assume that initially, at $t < 0$, the electron density N has a value of N_1, and, correspondingly, E_F and Ω are E_{F1} and Ω_1. A transverse magnetic (TM) surface plasmon with frequency ω_1 propagates along the graphene sheet in the x direction (Fig. 1). The electromagnetic field of the plasmon has three components: E_x, E_y, and H_z. The tangential electric field E_x can be written as

$$E_x(x, y, t) = E_0 e^{i\omega_1 t - ih_1 x - \varkappa_1 |y|}, \tag{2}$$

where the propagation (h_1) and decay ($\varkappa_1$) constants are defined by substituting ω_1 and Ω_1 to the dispersion relations for graphene plasmons [39]:

$$h(\omega) = \frac{\omega}{c}\sqrt{\varepsilon}\sqrt{1 + \frac{\varepsilon\omega^2}{\Omega^2}}, \quad \varkappa(\omega) = \frac{\varepsilon\omega^2}{c\Omega}. \tag{3}$$

There is a surface current density $j_x = \sigma_1 E_x(x, 0, t)$, with $\sigma_1 = \sigma(\omega_1, \Omega_1)$ [Eq. (1)], associated with the plasmon that leads to a discontinuity in the plasmon's magnetic field across the graphene sheet: H_z jumps from $H_0 = i\omega_1 E_0/(c\varkappa_1)$ at $y = 0^-$ to $-H_0$ at $y = 0^+$.

The time-averaged plasmon energy (per unit surface area) $W_0 = W_E + W_H + W_k$ consists of the energies of its electric (W_E) and magnetic (W_H) fields and the kinetic energy W_k of the oscillating carriers:

$$W_{E,H} = \frac{E_0^2 \varepsilon}{4\pi\varkappa_1}\left(\frac{h_1^2}{\varkappa_1^2} \pm 1\right), \quad W_k = \frac{2\pi |j_0|^2}{c\Omega_1}, \tag{4}$$

where $j_0 = \sigma_1 E_0$, and we adopted that the real field is twice the real part of the complex field.

At small frequencies, $\omega_1/\Omega_1 \lesssim 1$, the plasmon is weakly localized and propagates with the phase velocity close to $c/\sqrt{\varepsilon}$. At large frequencies, $\omega_1/\Omega_1 \gg 1$, the plasmon is strongly confined to the sheet and its phase velocity $\omega_1/h_1 \approx c\Omega_1/(\omega_1\varepsilon) \ll c/\sqrt{\varepsilon}$ (the quasistatic or nonretarded limit) [39]. In this limit, the magnetic energy is negligible, $W_H \ll W_E$, and the plasmon energy consists mainly of the electric and kinetic parts, $W_k \approx W_E$.

At $t = 0$, the carrier density grows instantly from N_1 to N_2 (Fig. 1) and, therefore, the Fermi level increases from E_{F1} to E_{F2}. This leads to a change in the parameter Ω from Ω_1 to Ω_2 in the graphene conductivity and, as a result, to temporal scattering of the initial surface plasmon.

To find the scattered fields at $t > 0$ we use the Maxwell equations

$$ih_1 E_y + \frac{\partial E_x}{\partial y} = \frac{1}{c}\frac{\partial H_z}{\partial t}, \tag{5a}$$

$$\frac{\partial H_z}{\partial y} = \frac{\varepsilon}{c}\frac{\partial E_x}{\partial t} + \frac{4\pi}{c}\left[j_x^{(b)} + j_x^{(n)}\right]\delta(y), \tag{5b}$$

$$ih_1 H_z = \frac{\varepsilon}{c}\frac{\partial E_y}{\partial t}, \tag{5c}$$

where $\delta(y)$ is the δ function and $j_x^{(b,n)}$ are the current densities of the "background" (that existed at $t < 0$) and "new" (created at $t = 0$) carriers, respectively. In Eq. (5), we took into account the invariance of the spatial dependence $e^{-ih_1 x}$ set by the initial plasmon in the translationally invariant along the x-axis system. The currents $j_x^{(b,n)}$ obey at $t > 0$ the time-domain Drude equations

$$\frac{\partial j_x^{(b)}}{\partial t} = \frac{c\Omega_1}{2\pi}E_x, \quad \frac{\partial j_x^{(n)}}{\partial t} = \frac{c(\Omega_2 - \Omega_1)}{2\pi}E_x. \tag{6}$$

Equations (5) and (6) are to be supplemented by initial conditions at $t = 0^+$. By integrating Eq. (5) over the infinitesimal jump time, we obtain continuity of the fields at the carrier density jump. It is reasonable to assume that current of the "background" electrons remains unchanged at the jump and the "new" electrons are born with zero current:

$$j_x^{(b)}(t = 0^+) = j_x^{(b)}(t = 0^-), \quad j_x^{(n)}(t = 0^+) = 0. \tag{7}$$

Equation (7) corresponds to physically reasonable conditions that the oscillation velocity of the "background" electrons cannot change instantaneously and the "new" electrons cannot acquire an oscillation velocity immediately after their creation. These conditions are analogous to those for three-dimensional time-varying plasmas [29,33]. The fields and current $j_x^{(b)}$ at $t = 0^-$ are given by the initial plasmon.

III. ANALYTICAL SOLUTION

To solve Eqs. (5) and (6) with the specified initial conditions, we apply the Laplace transform technique [30,33]. In the Laplace domain, we arrive at inhomogeneous Helmholtz equations for the transform $\tilde{E}_x(x, y, s)$ of $E_x(x, y, t)$ (s is the Laplace variable) in the $y < 0$ and $y > 0$ regions with boundary conditions of continuity of $\tilde{E}_x$ and a given jump of $\partial\tilde{E}_x/\partial y$ at $y = 0$. By solving this boundary problem, we obtain

$$\tilde{E}_x(x, y, s) = \frac{E_x(x, y, 0)}{s - i\omega_1} + A(s)e^{-ih_1 x - \varkappa(s)|y|}, \tag{8}$$

where $\varkappa(s) = \sqrt{h_1^2 + \varepsilon s^2/c^2}$ and

$$A(s) = -\frac{\varkappa(s)(\Omega_2 - \Omega_1)E_0}{\Omega_2(s - i\omega_1)D(s)}, \quad D(s) = \varkappa(s) + \frac{\varepsilon s^2}{c\Omega_2}. \tag{9}$$

The first term on the right-hand side of Eq. (8) is a forced response and its inverse Laplace transform contributes to $E_x(x, y, t)$ beginning at $t = 0^+$ at any y. This contribution is identical to the field of the initial plasmon given by Eq. (2).

The second term on the right-hand side of Eq. (8) is a free-wave response. The inverse Laplace transform of this term vanishes for $t < |y|/c$ because of the presence of $\exp[st - \varkappa(s)|y|]$ in the integrand of the inversion integral (the integration path in this case should be closed on the right half-plane of the complex variable s). For $t > |y|/c$, the integration path should be closed on the left half-plane, thereby switching on the free-wave contribution. Thus, the region of transient processes starts to expand from $y = 0$ beginning at $t = 0^+$ into both half-spaces $y \lessgtr 0$ with the velocity $c/\sqrt{\varepsilon}$.

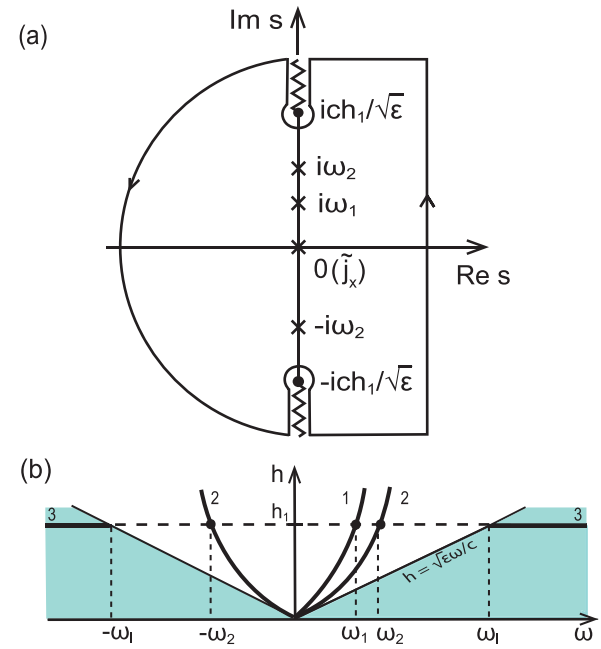

FIG. 2. (a) Closed path for contour integration in the s plane. The crosses indicate poles (the pole at $s = 0$ is only for $\tilde{j}_x$), the zigzag lines show branch cuts. (b) Kinematic diagram illustrating the frequency shifting. The lines 1 and 2 are the dispersion curves for the plasmons at densities N_1 and N_2, respectively. The shaded region shows the continuous spectrum for bulk waves. The lines 3 define the spectrum of the transient radiation.

At $t \to \infty$ the electromagnetic fields separate into two parts: surface plasmons localized in the vicinity of the graphene sheet and transient bulk radiation going to $y \to \pm\infty$. For the evaluation of the plasmons and angular distribution of the outgoing radiation, the closed integration path in the inverse Laplace transform of the second term in Eq. (8) is chosen as shown in Fig. 2(a). The integration path lies in the Riemann sheet of the complex s plane where $\mathrm{Re}\,\varkappa(s)$ is positive to ensure evanescence of the fields at $y \to \pm\infty$. The branch cuts [due to the double-valued function $\varkappa(s)$] run along the imaginary axis from the branch points $\pm ich_1/\sqrt{\varepsilon}$ to infinity.

The residue of $A(s)$ at the pole $s = i\omega_1$ cancels the forced response. The surface plasmons are described by the residues at the poles where $D(s) = 0$. This equation has two roots $s = \pm i\omega_2$ with

$$\omega_2 = \frac{\Omega_2}{\sqrt{2\varepsilon}}\left[\left(1 + 4c^2h_1^2/\Omega_2^2\right)^{1/2} - 1\right]^{1/2}. \tag{10}$$

With fixed spatial dependence $e^{-ih_1 x}$, the roots $\pm i\omega_2$ correspond to the plasmons propagating in the $+x$ direction

(transmitted) and $-x$ direction (reflected). The plasmons are frequency upshifted ($\omega_2 > \omega_1$) as illustrated by Fig. 2(b). By evaluating the residues at $s = \pm i\omega_2$, the amplitudes of the transmitted and reflected plasmons are given by

$$E_x^{t,r} = \frac{\varepsilon\omega_2^3(\Omega_2 - \Omega_1)}{\Omega_2(\omega_2 \mp \omega_1)\left(2\varepsilon\omega_2^2 + \Omega_2^2\right)}E_0. \tag{11}$$

The plasmon energies can be calculated by using Eqs. (4) and (11).

The transient radiation is described by the integrals along the branch cuts [Fig. 2(a)]. These integrals give the expansion of the transient field into plane waves. The frequency ω of an outgoing partial plane wave is related to the angle of propagation θ measured from the x axis as $\omega(\theta) = ch_1/(\sqrt{\varepsilon}\cos\theta)$. The waves with positive frequencies propagate at angles $-\pi/2 < \theta < \pi/2$, the waves with negative frequencies propagate at angles $\pi/2 < |\theta| < \pi$. All transient radiation is frequency upshifted with respect to the initial plasmon [Fig. 2(b)]. The partial waves of the lowest frequency $|\omega| = \omega_l = ch_1/\sqrt{\varepsilon}$ propagate along the graphene sheet, whereas the higher-frequency waves propagate in the normal to the sheet directions ($|\omega| \to \infty$ at $\theta \to \pm\pi/2$). The energy $W_{\rm rad}$ radiated from a unit area of the graphene sheet is obtained by integration of the energy flux through the unit area parallel to the sheet and can be expressed in terms of its angular density $w(\theta)$ as

$$W_{\rm rad} = \int_{-\pi}^{\pi} d\theta w(\theta), \quad w(\theta) = \frac{c^2h_1}{4\pi^2}\frac{|A[i\omega(\theta)]|^2}{\cos^2\theta}. \tag{12}$$

To find the currents in the graphene sheet after the carrier density jump, we derive the transforms of the currents from Eqs. (6) and (7) as

$$\tilde{j}_x^{(b)} = \frac{c\Omega_1}{2\pi s}\tilde{E}_x + \frac{1}{s}j_x^{(b)}(0^-), \quad \tilde{j}_x^{(n)} = \frac{c(\Omega_2 - \Omega_1)}{2\pi s}\tilde{E}_x, \tag{13}$$

where the transform $\tilde{E}_x(x, y, s)$ is taken at $y = 0$. The residues of Eq. (13) at the poles $s = \pm i\omega_2$ define the net current $j_x = j_x^{(b)} + j_x^{(n)}$ associated with the transmitted and reflected plasmons: $j_x^{t,r} = \pm\sigma_2 E_x^{t,r} e^{\pm i\omega_2 t - ih_1 x}$, where $\sigma_2 = -ic\Omega_2/(2\pi\omega_2)$.

The residues of $\tilde{j}_x^{(b,n)}$ at $s = 0$ [Eq. (13) and Fig. 2(a)] give the oppositely directed dc currents of the "background" and "new" electrons:

$$j_x^{(b,dc)} = -j_x^{(n,dc)} = \sigma_1\frac{\Omega_2 - \Omega_1}{\Omega_2}E_0 e^{-ih_1 x}. \tag{14}$$

Due to a zero net current [$j_x^{(b,dc)} + j_x^{(n,dc)} = 0$] this two-stream carrier motion does not generate any magnetic field.

IV. ANALYSIS AND RESULTS

A. Transmitted and reflected plasmons

Figure 3(a) shows the ratio of the final and initial plasmon frequencies ω_2/ω_1 as a function of Ω_2/Ω_1. The ratio increases with Ω_2/Ω_1; the closer the initial plasmon to the quasistatic regime (the higher ω_1/Ω_1), the larger the increase of ω_2/ω_1. For $\omega_1/\Omega_1 \gtrsim 10$, $\omega_2/\omega_1 \approx \sqrt{\Omega_2/\Omega_1}$, as in Ref. [34] (see also Sec. IV E). Since ω_2/ω_1 increases with Ω_2/Ω_1 slower than Ω_2/Ω_1, the relative plasmon frequency ω_2/Ω_2 decreases with

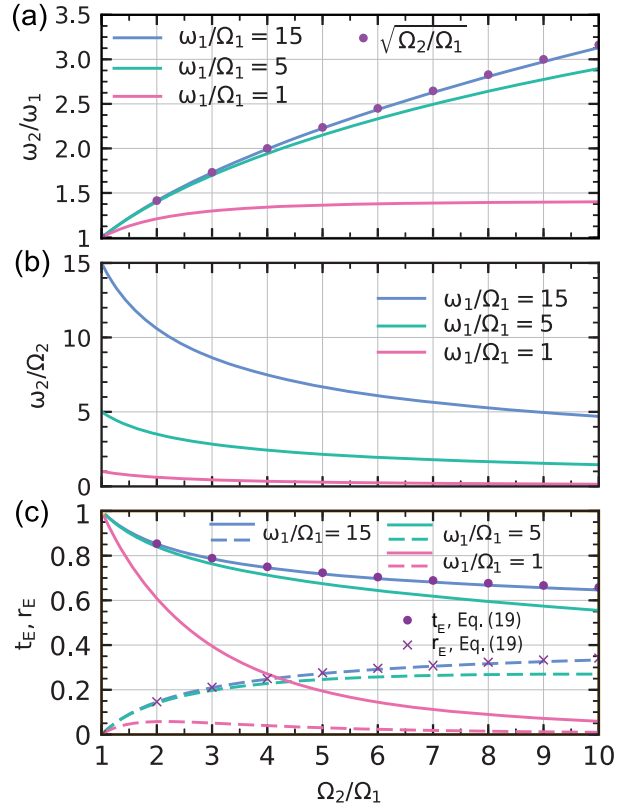

FIG. 3. Frequency ω_2 of the excited plasmons relative to (a) the initial frequency ω_1 and (b) to the frequency parameter Ω_2 as functions of Ω_2/Ω_1 for different ω_1/Ω_1. (c) Transmission (solid) and reflection (dashed) coefficients t_E, r_E as functions of Ω_2/Ω_1 for different ω_1/Ω_1. In (a) and (c), the dots and crosses show the dependencies in the quasistatic limit, Eqs. (18) and (19).

Ω_2/Ω_1 [Fig. 3(b)] and the excited plasmons become less confined.

Figure 3(c) shows the transmission $t_E = E_x^t/E_0$ and reflection $r_E = E_x^r/E_0$ coefficients, calculated by using Eq. (11), as functions of Ω_2/Ω_1. The transmission coefficient decreases monotonically with Ω_2/Ω_1; the smaller ω_1/Ω_1, the steeper the decrease. The reflection coefficient has a maximum whose position shifts to larger values with increasing ω_1/Ω_1. For a fixed Ω_2/Ω_1, r_E is larger for larger ω_1/Ω_1. For $\omega_1/\Omega_1 \gtrsim 10$, t_E and r_E approach the quasistatic dependencies derived below in Sec. IV E.

In general, according to Figs. 3(a) and 3(c), the quasistatic approximation works very well even for moderate values $\omega_1/\Omega_1 \gtrsim 10$.

B. Transient radiation

The transient radiation with frequency $\omega(\theta) = \omega_l/\cos\theta$ [Fig. 4(a)] propagates from the graphene sheet to $y \to \pm\infty$ and its angular distribution is described by Eq. (12). Figure 4(b) shows typical angular distributions. The weakly localized plasmon, $\omega_1/\Omega_1 = 1$, produces a rather narrow radiation peak at a small angle. The strongly localized plasmon, $\omega_1/\Omega_1 = 15$, emits in a broader angular range, including the angles $|\theta| > 90^\circ$.

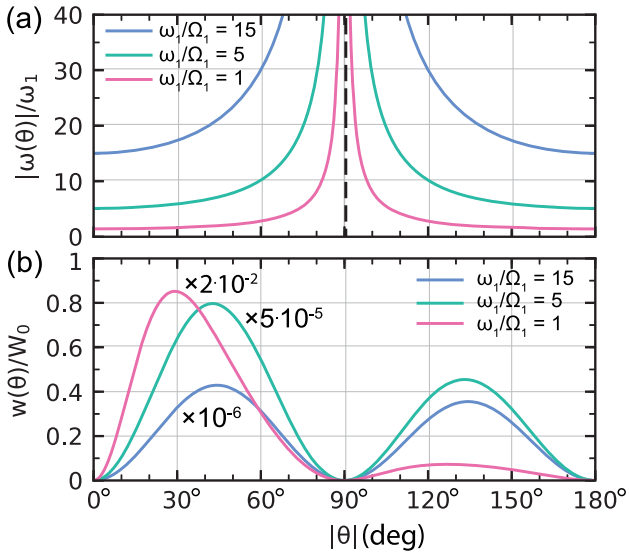

FIG. 4. Far-field angular distributions of (a) the frequency $\omega(\theta)$ and (b) the radiated energy $w(\theta)/W_0$ for $\Omega_2/\Omega_1 = 2$ and different ω_1/Ω_1. In (b), the values are to be multiplied by the indicated factors.

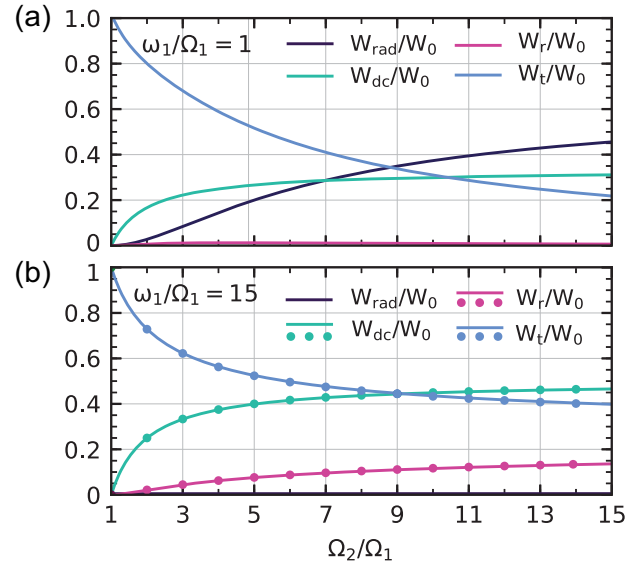

FIG. 5. Energy distribution as a function of Ω_2/Ω_1 for (a) $\omega_1/\Omega_1 = 1$ and (b) $\omega_1/\Omega_1 = 15$. In (b), the dots show the dependencies in the quasistatic limit, Eq. (20).

C. Two-stream dc motion of carriers

The dc currents of the "background" and "new" electrons, described by Eq. (14), totally compensate each other in every point of the graphene sheet, thus producing a zero net current and zero magnetic field. Nevertheless, these "hidden" currents consume a part of the initial plasmon energy in the form of the kinetic energy of carriers. This energy can be calculated by substituting Eq. (14) to the formula similar to Eq. (4) and expressed through the kinetic energy W_k of the initial plasmon [Eq. (4)] as

$$W_{\rm dc} = (1 - \Omega_1/\Omega_2)W_k. \tag{15}$$

According to Eq. (15), $W_{\rm dc}$ is restricted from above by W_k. Nevertheless, $W_{\rm dc}$ can comprise up to a half of W_0 at $\omega_1/\Omega_1 \gg 1$ (quasistatic regime) and $\Omega_2/\Omega_1 \gg 1$ (large carrier density jumps).

D. Energy balance

The energy of the initial plasmon (W_0) transforms into the energies of the transmitted (W_t) and reflected (W_r) plasmons, the energy of the transient outgoing radiation ($W_{\rm rad}$), and the energy of the two-stream dc motion of carriers ($W_{\rm dc}$):

$$W_0 = W_t + W_r + W_{\rm rad} + W_{\rm dc}. \tag{16}$$

Figure 5 shows the energy distribution as a function of the carrier density jump for weakly ($\omega_1/\Omega_1 = 1$) and strongly ($\omega_1/\Omega_1 = 15$) confined initial plasmons. The energy of a weakly confined plasmon [Fig. 5(a)] is mainly divided between the transmitted plasmon, the dc motion, and the bulk radiation. For large density jumps, $W_{\rm rad}$ becomes dominating. The smaller is ω_1/Ω_1, the larger is $W_{\rm rad}$, and the smaller is $W_{\rm dc}$. The energy of the reflected plasmon is negligible for any carrier density jump. The energy of a strongly confined plasmon [Fig. 5(b)] is mainly divided between the transmitted plasmon and dc motion, although the energy of the reflected plasmon becomes substantial at large Ω_2/Ω_1.

E. Scattering in quasistatic regime

In the practically most important case of a strongly confined (with $\omega_1/\Omega_1 \gg 1$) initial plasmon, the scattering problem can be solved in a simpler (approximate) way, without using the general approach of Sec. III. In the quasistatic limit $\omega_1/\Omega_1 \gg 1$, the magnetic field of the plasmon is negligible, $|H_0/E_0| = \Omega_1/(\varepsilon\omega_1) \ll 1$, and temporal discontinuity produces only very weak bulk radiation [Fig. 5(b)]. Thus, we can write the electric field at $t > 0$ as a superposition of the transmitted and reflected plasmons,

$$E_x(x, y, t) = E_0(t_E e^{i\omega_2 t} + r_E e^{-i\omega_2 t})e^{-ih_1 x - \varkappa_1|y|}. \tag{17}$$

In Eq. (17), the spatial structure of the plasmons is set by the initial plasmon [Eq. (2)]. By using Eq. (3), this spatial invariance immediately gives

$$\omega_2/\omega_1 = \gamma, \quad \gamma = \sqrt{\Omega_2/\Omega_1}. \tag{18}$$

The results given by Eq. (18) for $\omega_1/\Omega_1 \gg 1$ agree well with accurate Eq. (10), see Fig. 3(a).

The currents at $t > 0$ can be obtained by substituting Eq. (17) to Eq. (6). By applying further the continuity of E_x and j_x at $t = 0$, we find

$$t_E = (1 + \gamma^{-1})/2, \quad r_E = (1 - \gamma^{-1})/2. \tag{19}$$

Equations (19) agree well with the general formulas Eq. (11) for $\omega_1/\Omega_1 \gg 1$, as seen from Fig. 3(c).

With Eqs. (19) in hand, the energies can be written as

$$W_{t,r} = W_0(1 \pm \gamma^{-1})^2/4, \quad W_{\rm dc} = W_0(1 - \gamma^{-2})/2, \tag{20}$$

with $W_0 = \varepsilon E_0^2/(\pi\varkappa_1)$. These approximate formulas work very well for $\omega_1/\Omega_1 \gtrsim 10$ (Fig. 5).

F. Comparison with other works

Formulas in Eq. (19) are different from those obtained within the similar approach for a carrier density decrease [36]:

$$t_E = (1+\gamma)/2, \quad r_E = (1-\gamma)/2. \tag{21}$$

The difference between Eqs. (19) and (21) can be explained by different initial conditions for the surface current—its continuity at an abrupt carrier density increase [Eq. (7)] and sudden reduction at a density decrease [36]. Thus, there are no universal formulas to describe both an increase ($\gamma > 1$) and decrease ($\gamma < 1$) of the carrier density, contrary to the view adopted in Refs. [34,35].

To compare our results with those in Refs. [34,35], we obtain from Eq. (19) the transmission (t_H) and reflection (r_H) coefficients in terms of the magnetic field:

$$t_H = (1+\gamma)/2, \quad r_H = (1-\gamma)/2. \tag{22}$$

These formulas differ by a factor of γ from the corresponding formulas in Ref. [34]:

$$|t_H| = (1+\gamma)/(2\gamma), \quad |r_H| = |1-\gamma|/(2\gamma). \tag{23}$$

The origin of the difference between Eqs. (22) and (23) is in incorrect initial conditions used in Ref. [34], as was explained in the Introduction.

Interestingly, the coefficients obtained in Ref. [35] coincide with Eq. (22). This justifies the applicability of the initial conditions in Ref. [35], in particular, the continuity of the magnetic field, to the case of a carrier density increase. Why can this continuity, being incorrect for a carrier density decrease [36], be used for an increase? The physical reason for this is the continuity of the surface current at a carrier density increase [Eq. (7)] and the zero net current [Eq. (14)] and magnetic field in the two-stream dc motion of carriers. Thus, our rigorous solution clarifies the applicability of the heuristic initial conditions in Ref. [35].

Despite the correctness of the transmission and reflection coefficients in Ref. [35] for a carrier density increase, it was incorrectly concluded that nonstationarity can amplify plasmons by imparting energy to them. Equation (22) indeed gives $t_H > 1$ for $\gamma > 1$, i.e., the magnetic field of the transmitted plasmon is larger than that of the initial plasmon. This, however, does not mean an amplification. The electric field of the transmitted plasmon decreases with γ: $t_E < 1$ for $\gamma > 1$, according to Eq. (19). As a result, the energy of the transmitted plasmon also decreases: $W_t < W_0$ for $\gamma > 1$, see Eq. (20). The increase of the plasmon's magnetic field with increasing carrier density can be explained by a decrease of the relative frequency ω_2/Ω_2 with γ (Fig. 3) and, as a result, a reduction in the plasmon confinement. Since the plasmon magnetic field is negligible in the quasistatic approximation, its increase practically does not contribute to the plasmon energy.

Finally, the considerations in Refs. [34] and [35] did not analyze currents in graphene and therefore completely missed the two-stream dc motion of carriers consuming the initial plasmon's energy (Sec. IV C).

V. CONCLUSION

To conclude, the temporal scattering of a surface plasmon on a doped graphene sheet by an abrupt increase of graphene's free-carrier density has been considered. An accurate analytical solution of the Maxwell equations supplemented by the time-domain Drude equations has been obtained by means of the Laplace transform technique. It has been shown that scattering gives rise to frequency-upshifted transmitted and reflected plasmons, frequency-upshifted bulk radiation, and peculiar two-stream dc motion of carriers. The two-stream motion arises due to different initial velocities of the background and newly created carriers at the temporal discontinuity. The motion carries zero net current and therefore does not generate a magnetic field. This mode, however, takes some energy of the initial plasmon. Thus, the energy of the transmitted and reflected plasmons and bulk radiation is smaller than the initial plasmon energy. This refutes the prediction of plasmon amplification in Ref. [35].

In the quasistatic regime, simple formulas for the amplitudes and energies of the transmitted and reflected plasmons, as well as for the energy of the dc carrier motion, have been obtained. In this regime, up to a half of the initial plasmon energy can be transformed into the two-stream dc motion of carriers: $W_{\rm dc} \approx W_0/2$ at $\Omega_2/\Omega_1 \gg 1$. The remaining energy is distributed between the transmitted and reflected plasmons. In particular, $W_t \approx W_r \approx W_0/4$ at $\Omega_2/\Omega_1 \gg 1$.

It has been also shown that there are no universal formulas to describe both an increase and decrease of the carrier density. If, for example, one needs to consider plasmon scattering on a rectangular temporal profile of the carrier density, the formulas of this work and Ref. [36] should be successively applied to the first and second time steps, respectively. Remarkably, both steps will reduce the plasmon energy.

ACKNOWLEDGMENT

This work was supported by the Ministry of Science and Higher Education of the Russian Federation, Project No. 3.3854.2017/4.6.

[1] D. Rodrigo, O. Limaj, D. Janner, D. Etezadi, F. J. Garcia de Abajo, V. Pruneri, and H. Altug, Mid-infrared plasmonic biosensing with graphene, Science **349**, 165 (2015).

[2] H. Hu, X. Yang, F. Zhai, D. Hu, R. Liu, K. Liu, Z. Sun, and Q. Dai, Far-field nanoscale infrared spectroscopy of vibrational fingerprints of molecules with graphene plasmons, Nat. Commun. **7**, 12334 (2016).

[3] T. Low and P. Avouris, Graphene plasmonics for terahertz to mid-infrared applications, ACS Nano **8**, 1086 (2014).

[4] D. A. Bandurin, D. Svintsov, I. Gayduchenko, S. G. Xu, A. Principi, M. Moskotin, I. Tretyakov, D. Yagodkin, S. Zhukov, T. Taniguchi, K. Watanabe, I. V. Grigorieva, M. Polini, G. N. Goltsman, A. K. Geim, and G. Fedorov, Resonant terahertz detection using graphene plasmons, Nat. Commun. **9**, 5392 (2018).

[5] T. Zhao, S. Gong, M. Hu, R. Zhong, D. Liu, X. Chen, P. Zhang, X. Wang, C. Zhang, P. Wu, and S. Liu, Coherent and tunable terahertz radiation from graphene surface plasmon polarirons excited by cyclotron electron beam, Sci. Rep. **5**, 16059 (2015).

[6] L. J. Wong, I. Kaminer, O. Ilic, J. D. Joannopoulos, and M. Soljačić, Towards graphene plasmon-based free-electron infrared to X-ray sources, Nat. Photonics **10**, 46 (2016).

[7] H. Yan, X. Li, B. Chandra, G. Tulevski, Y. Wu, M. Freitag, W. Zhu, P. Avouris, and F. Xia, Tunable infrared plasmonic devices using graphene/insulator stacks, Nat. Nanotechnol. **7**, 330 (2012).

[8] S. Qu, C. Ma, and H. Liu, Tunable graphene-based hybrid plasmonic modulators for subwavelength confinement, Sci. Rep. **7**, 5190 (2017).

[9] R. Hao, Z. Ye, X. Peng, Y. Gu, J. Y. Jiao, H. Zhu, W. E. I. Sha, and E. Li, Highly efficient graphene-based optical modulator with edge plasmonic effect, IEEE Photonics J. **10**, 4500807 (2018).

[10] A. N. Grigorenko, M. Polini, and K. S. Novoselov, Graphene plasmonics, Nat. Photonics **6**, 749 (2012).

[11] S. J. B. Yoo, Wavelength conversion technologies for WDM network applications, J. Lightwave Technol. **14**, 955 (1996).

[12] A. E. Willner, S. Khaleghi, M. R. Chitgarha, and O. F. Yilmaz, All-optical signal processing, J. Lightwave Technol. **32**, 660 (2014).

[13] S. F. Preble, Q. Xu, and M. Lipson, Changing the colour of light in a silicon resonator, Nat. Photonics **1**, 293 (2007).

[14] P. Dong, S. F. Preble, J. T. Robinson, S. Manipatruni, and M. Lipson, Inducing Photonic Transitions between Discrete Modes in a Silicon Optical Microcavity, Phys. Rev. Lett. **100**, 033904 (2008).

[15] T. Tanabe, M. Notomi, H. Taniyama, and E. Kuramochi, Dynamic Release of Trapped Light from an Ultrahigh-Q Nanocavity via Adiabatic Frequency Tuning, Phys. Rev. Lett. **102**, 043907 (2009).

[16] J. Upham, Y. Tanaka, T. Asano, and S. Noda, On-the-fly wavelength conversion of photons by dynamic control of photonic waveguides, Appl. Phys. Express **3**, 062001 (2010).

[17] T. Kampfrath, D. M. Beggs, T. P. White, A. Melloni, T. F. Krauss, and L. Kuipers, Ultrafast adiabatic manipulation of slow light in a photonic crystal, Phys. Rev. A **81**, 043837 (2010).

[18] D. M. Beggs, T. F. Krauss, L. Kuipers, and T. Kampfrath, Ultrafast Tunable Optical Delay Line Based on Indirect Photonic Transitions, Phys. Rev. Lett. **108**, 033902 (2012).

[19] T. Li, L. Luo, M. Hupalo, J. Zhang, M. C. Tringides, J. Schmalian, and J. Wang, Femtosecond Population Inversion and Stimulated Emission of Dense Dirac Fermions in Graphene, Phys. Rev. Lett. **108**, 167401 (2012).

[20] J. C. Johannsen, S. Ulstrup, F. Cilento, A. Crepaldi, M. Zacchigna, C. Cacho, I. C. E. Turcu, E. Springate, F. Fromm, C. Raidel, T. Seyller, F. Parmigiani, M. Grioni, and P. Hofmann, Direct View of Hot Carrier Dynamics in Graphene, Phys. Rev. Lett. **111**, 027403 (2013).

[21] I. Gierz, J. C. Petersen, M. Mitrano, C. Cacho, I. C. E. Turcu, E. Springate, A. Stöhr, A. Köhler, U. Starke, and A. Cavalleri, Snapshots of non-equilibrium Dirac carrier distributions in graphene, Nat. Mater. **12**, 1119 (2013).

[22] G. X. Ni, L. Wang, M. D. Goldflam, M. Wagner, Z. Fei, A. S. McLeod, M. K. Liu, F. Keilmann, B. Özyilmaz, A. H. Castro Neto, J. Hone, M. M. Fogler, and D. N. Basov, Ultrafast optical switching of infrared plasmon polaritons in high-mobility graphene, Nat. Photonics **10**, 244 (2016).

[23] A. Tomadin, S. M. Hornett, H. I. Wang, E. M. Alexeev, A. Candini, C. Coletti, D. Turchinovich, M. Kläui, M. Bonn, F. H. L. Koppens, E. Hendry, M. Polini, and K.-J. Tielrooij, The ultrafast dynamics and conductivity of photoexcited graphene at different Fermi energies, Sci. Adv. **4**, eaar5313 (2018).

[24] M. Baudisch, A. Marini, J. D. Cox, T. Zhu, F. Silva, S. Teichmann, M. Massicotte, F. Koppens, L. S. Levitov, F. J. Garcia de Abajo, and J. Biegert, Ultrafast nonlinear optical response of Dirac fermions in graphene, Nat. Commun. **9**, 1018 (2018).

[25] F. R. Morgenthaler, Velocity modulation of electromagnetic waves, IRE Trans. Microwave Theory Tech. **6**, 167 (1958).

[26] C.-L. Jiang, Wave propagation and dipole radiation in a suddenly created plasma, IEEE Trans. Antennas Propag. **23**, 83 (1975).

[27] D. K. Kalluri, *Electromagnetics of Time Varying Complex Media: Frequency and Polarization Transformer*, 2nd ed. (CRC Press, Boca Raton, FL, 2010).

[28] B. W. Plansinis, W. R. Donaldson, and G. P. Agrawal, Spectral splitting of optical pulses inside a dispersive medium at a temporal boundary, IEEE J. Quantum Electron. **52**, 1 (2016).

[29] K. Qu, Q. Jia, M. R. Edwards, and N. J. Fisch, Theory of electromagnetic wave frequency upconversion in dynamic media, Phys. Rev. E **98**, 023202 (2018).

[30] M. I. Bakunov and S. N. Zhukov, Conversion of a surface electromagnetic wave at the boundary of a time-varying plasma, Plasma Phys. Rep. **22**, 649 (1996).

[31] M. I. Bakunov, V. B. Gildenburg, S. N. Zhukov, and N. A. Zharova, Adiabatic frequency shifting of a surface wave guided by a time-varying plasma structure, Phys. Plasmas **7**, 1035 (2000).

[32] M. I. Bakunov, A. V. Maslov, and S. N. Zhukov, Time-dependent scattering of a standing surface plasmon by rapid ionization in a semiconductor, Opt. Lett. **25**, 926 (2000).

[33] M. I. Bakunov, A. V. Maslov, and S. N. Zhukov, Scattering of a surface plasmon polariton by rapid plasma creation in a semiconductor slab, J. Opt. Soc. Am. B **16**, 1942 (1999).

[34] G. A. Menendez and B. Maes, Time reflection and refraction of graphene plasmons at a temporal discontinuity, Opt. Lett. **42**, 5006 (2017).

[35] J. Wilson, F. Santosa, M. Min, and T. Low, Temporal control of graphene plasmons, Phys. Rev B **98**, 081411(R) (2018).

[36] A. V. Maslov and M. I. Bakunov, Temporal scattering of a graphene plasmon by a rapid carrier density decrease, Optica **5**, 1508 (2018).

[37] F. H. L. Koppens, D. E. Chang, and F. J. Garcia de Abajo, Graphene plasmonics: A platform for strong light-matter interactions, Nano Lett. **11**, 3370 (2011).

[38] Y. V. Bludov, A. Ferreira, N. M. R. Peres, and M. I. Vasilevskiy, A primer on surface plasmon-polariton in graphene, Int. J. Mod. Phys B **27**, 1341001 (2013).

[39] M. Jablan, H. Buljan, and M. Soljačić, Plasmonics in graphene at infrared frequencies, Phys. Rev. B **80**, 245435 (2009).